SCIENCE CHINA
Mathematics

• ARTICLES •

https://doi.org/10.1007/s11425-025-2550-x

A third-order accurate, linear energy stable BDF3 numerical scheme for the nonlocal Cahn-Hilliard equation

Qiumei Huang[1], Cheng Wang[2] & Nan Zheng[3,*]

[1]*School of Mathematics, Statistics and Mechanics, Beijing University of Technology, Beijing* 100124*, China;*
[2]*Department of Mathematics, The University of Massachusetts, North Dartmouth, MA* 02747*, USA;*
[3]*Department of Applied Mathematics, The Hong Kong Polytechnic University, Hong Kong, China*

*Email: qmhuang@bjut.edu.cn, cwang1@umassd.edu, znan*2017@163*.com*

Received July 11, 2025; accepted January 30, 2026; published online May 6, 2026

Abstract The primary challenge in designing a third-order energy-stable numerical method for the nonlocal Cahn-Hilliard equation is associated with handling the expansive concave term. We overcome this difficulty by combining it with the constant L^2 diffusion term under the diffusivity condition and employing an implicit treatment to ensure a theoretical stability analysis. In this paper, we propose and analyze a third-order accurate in time, linear stabilized numerical scheme for the nonlocal Cahn-Hilliard equation. A linearized backward differentiation formula (third-order backward differentiation formula) temporal discretization is applied, combined with the Fourier pseudo-spectral spatial discretization. The nonlinear term is approximated by an explicit extrapolation, and a third-order accurate Douglas-Dupont regularization term is added in the numerical system. With the help of this artificial regularization, a rough energy stability analysis is derived, in which a lower bound of the regularization parameter is required, dependent on the maximum norm bound of the numerical solution. The convergence analysis and error estimates are conducted, and an application of the inverse inequality recovers this functional bound. A novel test function for the error equation is taken in the form of a discrete temporal derivative, and such a test function plays a crucial role in the optimal convergence rate. Some numerical experiments, including both the convergence tests and simulation results of long-time coarsening process, are presented to demonstrate the robustness of the proposed third-order method.

Keywords nonlocal Cahn-Hilliard equation, third-order backward differentiation formula, modified energy stability analysis, convergence analysis, error estimate

MSC(2020) 35Q99, 65M12, 65M15, 65M70

Citation: Huang Q M, Wang C, Zheng N. A third-order accurate, linear energy stable BDF3 numerical scheme for the nonlocal Cahn-Hilliard equation. Sci China Math, 2026, 69, https://doi.org/10.1007/s11425-025-2550-x

1 Introduction

The nonlocal Cahn-Hilliard (NCH) equation has attracted increasing attention in various areas, ranging from chemistry and material science to finance and image processing. Over $\Omega = \prod_{i=1}^{d}(-X_i, X_i)$, a

* Corresponding author

© Science China Press 2026

rectangular domain in $\mathbb{R}^d$, such a mathematical model is the H^{-1} gradient flow with respect to the following free energy functional, in which nonlocal interaction effects play an essential role [1–5]:

$$E(\phi) = \int_\Omega \left(\frac{1}{4}\phi^4 - \frac{1}{2}\phi^2 + \frac{\varepsilon^2}{4} \int_\Omega J(\boldsymbol{x}-\boldsymbol{y})(\phi(\boldsymbol{x}) - \phi(\boldsymbol{y}))^2 \, d\boldsymbol{y} \right) d\boldsymbol{x}, \tag{1.1}$$

where $\varepsilon > 0$ is an interfacial parameter. In more detail, the kernel function J is required to satisfy the following conditions [9, 23]:

(a) $J(\boldsymbol{x}) \geqslant 0$ for any $\boldsymbol{x} \in \Omega$;
(b) J is integrable in Ω and $\int_\Omega J(\boldsymbol{x})d\boldsymbol{x} > 0$;
(c) J is even, i.e., $J(\boldsymbol{x}) = J(-\boldsymbol{x})$ for any $\boldsymbol{x} \in \mathbb{R}^d$;
(d) J is Ω-periodic;
(e) $\frac{1}{2}\int_\Omega J(\boldsymbol{x})|\boldsymbol{x}|^2 d\boldsymbol{x} = 1$ (a finite second moment).

Subsequently, a nonlocal linear operator is defined as follows, based on the nonlocal free energy:

$$\mathcal{L} : \psi(\boldsymbol{x}) \mapsto \int_\Omega J(\boldsymbol{x}-\boldsymbol{y})(\psi(\boldsymbol{x}) - \psi(\boldsymbol{y}))d\boldsymbol{y}, \quad \text{so that } \mathcal{L}\psi = (J*1)\psi - J*\psi$$

with

$$(J*\psi)(\boldsymbol{x}) = \int_\Omega J(\boldsymbol{x}-\boldsymbol{y})\psi(\boldsymbol{y})d\boldsymbol{y} = \int_\Omega J(\boldsymbol{y})\psi(\boldsymbol{x}-\boldsymbol{y})d\boldsymbol{y} \quad \text{(a periodic convolution)}.$$

Meanwhile, a direct calculation gives an equivalent form of the free energy (1.1) as

$$E(\phi) = \int_\Omega F(\phi)d\boldsymbol{x} + \frac{\varepsilon^2}{2}(\mathcal{L}\phi, \phi)_{L^2}, \quad F(\phi) = \frac{1}{4}\phi^4 - \frac{1}{2}\phi^2. \tag{1.2}$$

As a result, the associated NCH equation is formulated as the H^{-1} gradient flow:

$$\partial_t \phi = \Delta\mu, \quad \mu := \delta_\phi E(\phi) = \phi^3 - \phi + \varepsilon^2\mathcal{L}\phi = \phi^3 - \phi + \varepsilon^2((J*1)\phi - J*\phi). \tag{1.3}$$

Moreover, the following diffusivity condition is imposed to enforce the well-posedness of the NCH equation:

$$\gamma_0 := \varepsilon^2(J*1) - 1 > 0. \tag{1.4}$$

Without this condition, the solution may exhibit some singular behaviors; see the related partial differential equation (PDF) analysis studies [3, 4, 6, 12, 18].

There have been extensive numerical studies of the NCH equation in recent years [2, 5, 10, 11, 31, 33, 34]. For any gradient flow equation, the free energy dissipation induced by the energetic variational formulation has always been a central issue in any numerical study. Several different approaches have been reported to preserve such an energy stability. Based on the convex-concave decomposition of the free energy (1.1), the convex splitting idea was applied to the NCH equation, and both the first- and second-order accurate numerical schemes have been analyzed in detail [14–16]. One special feature of the convex splitting approach is its implicit treatment of the nonlinear term, which comes from the convexity of the nonlinear energy part.

Because of the numerical challenges in the implementation of a nonlinearly implicit algorithm, the linearized and energy stable numerical scheme becomes more and more popular. In particular, the stabilized numerical approach, which treats the highest-order diffusion term implicitly while updating the nonlinear and concave terms explicitly, combined with an artificial regularization term, turns out to be a natural choice. For the standard local Cahn-Hilliard equation, the stabilized linear numerical schemes have been analyzed in detail [19–21, 29], in both the first and second accuracy orders (in time). In terms of the NCH equation, two stabilized linear semi-implicit schemes were proposed in [9], following a similar numerical design. In such a framework, a maximum norm bound of the numerical solution needs to be derived, so that a lower bound for the artificial regularization parameter enforces the energy stability at a theoretical level. If the standard local CH equation is considered, such a maximum norm bound can be established with the help of the surface diffusion; the related theoretical techniques have been reported

in [19–21]. Meanwhile, if the diffusion operator is replaced by a nonlocal version (as given by (1.3)), a global-in-time maximum norm bound would face a serious theoretical difficulty, due to the fact that the nonlocal diffusion term only corresponds to an L^2 regularity, in comparison with the H^1 regularity of the local diffusion operator. Instead, a local-in-time convergence analysis has to be performed, and the inverse inequality is needed to establish the corresponding energy stability estimate for the NCH equation; see the detailed analysis in [23–25]. Moreover, to further improve computational efficiency, various high-order time-stepping approaches have been developed for the Cahn-Hilliard equation [22, 26, 30].

On the other hand, all the existing stabilized linear numerical schemes have been only in the first or second temporal accuracy orders, for both the local and nonlocal CH models. In this paper, we propose a third-order accurate in time, stabilized linear scheme for the NCH equation, and theoretically establish the energy stability and convergence analysis. The temporal discretization is based on the third-order backward differentiation formula (BDF3) method. In the chemical potential expansion, the nonlinear term is approximated by a third-order accurate explicit extrapolation formula, following the stabilization idea. Meanwhile, the primary challenge in the numerical design of a third-order accurate and energy stable method is focused on the expansive concave term. If such a term is also approximated by an explicit extrapolation formula, a theoretical justification of the energy stability would face a serious difficulty, due to its long stencil nature. To overcome this difficulty, we combine the expansive concave term and the constant L^2 term in the diffusion part, and make use of the diffusivity condition (1.4). In turn, an implicit treatment is applied to such a combined constant multiple term, which plays an essential role in the theoretical analysis. Meanwhile, the explicit extrapolation becomes a natural choice for the convolution term, for the sake of unique solvability. Due to the smoothness of the convolution kernel function, the additional numerical dissipation in the temporal derivative term is able to balance such an explicit extrapolation in the energy stability analysis. Moreover, a third-order artificial regularization term, in the form of $A\Delta_N(\phi^{n+1} - 2\phi^n + \phi^{n-1})$, is added to the numerical method to ensure an energy stability analysis.

With a careful estimate in the discrete H^{-1} space, the energy stability of the proposed scheme can be derived, in terms of a modified energy, composed of the original energy functional and a few numerical correction terms. In more detail, such a modified energy stability analysis is associated with a lower bound for the artificial regularization parameter, dependent on the maximum norm of the numerical solution at the current and previous time steps, as well as the next time step. Meanwhile, a global-in-time ℓ^∞ bound of the numerical solution is not theoretically available, due to the lack of regularity for the nonlocal diffusion part. To overcome this difficulty, we perform an optimal rate convergence analysis of the stabilized third-order BDF3 scheme, and an application of the inverse inequality is applied to justify this ℓ^∞ bound. Thanks to the third-order accuracy in time, a higher-order asymptotic consistency analysis is not needed in the error estimate, which comes from the fact that the leading order truncation error is able to recover the maximum norm bound of the numerical solution. Because of the long temporal stencil in the BDF3 discretization, a standard H^{-1} error analysis would not be able to bring the desired result. Instead, an alternate test function, in the form of the discrete temporal difference between the numerical errors, is taken in the H^{-1} space, in comparison with the standard H^{-1} error estimate reported in [23] for the first-order scheme. Such a theoretical approach would provide a temporal difference between two associated error energy norms, and the convexity of the nonlinear terms also plays an important role. Subsequently, by making use of the derived convergence estimate, a uniform ℓ^∞ bound of the numerical solution becomes available, with the help of the inverse inequality. Therefore, the *a priori* assumption is recovered, so that the lower bound is derived for the stabilization constant for the energy stability analysis.

The rest of this paper is organized as follows. In Section 2, the stabilized BDF3 scheme is proposed, combined with the Fourier pseudo-spectral spatial discretization, and a modified energy stability is derived, under an ℓ^∞ bound assumption of the numerical solution. Subsequently, the convergence analysis and error estimates are provided in Section 3. In Section 4, some numerical results are presented to demonstrate the robustness and high-order accuracy of the proposed numerical scheme. Finally, some concluding remarks are given in Section 5.

2 The numerical scheme and the energy stability analysis

2.1 Fourier pseudo-spectral spatial approximation

The two-dimensional (2-D) Fourier spectral collocation discretization is considered; an extension to the three-dimensional (3-D) case turns out to be straightforward. Let N_x and N_y denote two integer numbers, and let the $N_x \times N_y$ mesh Ω_h of the domain $\Omega = (-X, X) \times (-Y, Y)$ become (x_i, y_j) with $x_i = -X + ih_x$, $y_j = -Y + jh_y$, $1 \leqslant i \leqslant N_x$, $1 \leqslant j \leqslant N_y$, where $h_x = 2X/N_x$ and $h_y = 2Y/N_y$ are the uniform mesh sizes in each direction. For simplicity of presentation, we take $h = \max\{h_x, h_y\}$, and the following index sets are introduced:

$$S_h = \{(i,j) \in \mathbb{Z}^2 \mid 1 \leqslant i \leqslant N_x,\ 1 \leqslant j \leqslant N_y\},$$
$$\widehat{S}_h = \left\{(k,l) \in \mathbb{Z}^2 \,\middle|\, -\frac{N_x}{2} + 1 \leqslant k \leqslant \frac{N_x}{2},\ -\frac{N_y}{2} + 1 \leqslant l \leqslant \frac{N_y}{2}\right\}.$$

In turn, all periodic grid functions on Ω_h are defined as

$$\mathcal{M}_h = \{f : \Omega_h \to \mathbb{R} \mid f_{i+mN_x, j+nN_y} = f_{ij} \text{ for any } (i,j) \in S_h \text{ and } (m,n) \in \mathbb{Z}^2\}.$$

For any two periodic grid functions $f, g \in \mathcal{M}_h$ and $\boldsymbol{f} = (f^1, f^2)^{\mathrm{T}}$, $\boldsymbol{g} = (g^1, g^2)^{\mathrm{T}} \in \mathcal{M}_h \times \mathcal{M}_h$, the discrete ℓ^2 inner product $\langle \cdot, \cdot \rangle$, discrete ℓ^2 norm $\|\cdot\|_2$, discrete ℓ^p norm $\|\cdot\|_p$ and discrete ℓ^∞ norm $\|\cdot\|_\infty$ can be defined as follows:

$$\langle f, g \rangle = h_x h_y \sum_{(i,j) \in S_h} f_{ij} g_{ij}, \quad \langle \boldsymbol{f}, \boldsymbol{g} \rangle = h_x h_y \sum_{(i,j) \in S_h} (f^1_{ij} g^1_{ij} + f^2_{ij} g^2_{ij}),$$
$$\|f\|_2 = \sqrt{\langle f, f \rangle}, \quad \|\boldsymbol{f}\|_2 = \sqrt{\langle \boldsymbol{f}, \boldsymbol{f} \rangle},$$
$$\|f\|_\infty = \max_{(i,j) \in S_h} |f_{ij}|, \quad \|\boldsymbol{f}\|_\infty = \max_{(i,j) \in S_h} \sqrt{|f^1_{ij}|^2 + |f^2_{ij}|^2},$$
$$\|f\|_p = (\langle |f|^p, \mathbf{1} \rangle)^{\frac{1}{p}}, \quad \|\boldsymbol{f}\|_p = (\langle |\boldsymbol{f}|^p, \mathbf{1} \rangle)^{\frac{1}{p}}, \quad 1 \leqslant p < +\infty.$$

Meanwhile, for any $f \in \mathcal{M}_h$, we introduce $\overline{f} := \frac{1}{|\Omega|} \langle f, 1 \rangle$ as the mean value of f. In particular, all the grid functions in $\mathcal{M}_h$ with mean zero are defined as $\mathcal{M}_h^0 = \{f \in \mathcal{M}_h \mid \langle f, 1 \rangle = 0\}$.

For any $f \in \mathcal{M}_h$, the 2-D discrete Fourier transform $\hat{f} = Pf$ is defined as [28, 32]

$$\hat{f}_{kl} = \sum_{(i,j) \in S_h} f_{ij} \exp\left(-\mathrm{i}\frac{k\pi}{X} x_i\right) \exp\left(-\mathrm{i}\frac{l\pi}{Y} y_j\right), \quad (k,l) \in \widehat{S}_h. \tag{2.1}$$

Conversely, f can be reconstructed through the corresponding inverse transform $f = P^{-1}\hat{f}$:

$$f_{ij} = \frac{1}{N_x N_y} \sum_{(k,l) \in \widehat{S}_h} \hat{f}_{kl} \exp\left(\mathrm{i}\frac{k\pi}{X} x_i\right) \exp\left(\mathrm{i}\frac{l\pi}{Y} y_j\right), \quad (i,j) \in S_h. \tag{2.2}$$

Let $\widehat{\mathcal{M}}_h = \{Pf \mid f \in \mathcal{M}_h\}$. The operators $\widehat{D}_x$ and $\widehat{D}_y$ on $\widehat{\mathcal{M}}_h$ are defined as

$$(\widehat{D}_x \hat{f})_{kl} = \left(\frac{k\pi\mathrm{i}}{X}\right) \hat{f}_{kl}, \quad (\widehat{D}_y \hat{f})_{kl} = \left(\frac{l\pi\mathrm{i}}{Y}\right) \hat{f}_{kl}, \quad (k,l) \in \widehat{S}_h.$$

In turn, the Fourier pseudo-spectral approximations to the first and second spatial derivatives become

$$D_x = P^{-1}\widehat{D}_x P, \quad D_y = P^{-1}\widehat{D}_y P, \quad D_x^2 = P^{-1}\widehat{D}_x^2 P, \quad D_y^2 = P^{-1}\widehat{D}_y^2 P.$$

Similarly, for any $f \in \mathcal{M}_h$ and $\boldsymbol{f} = (f^1, f^2)^{\mathrm{T}} \in \mathcal{M}_h \times \mathcal{M}_h$, the discrete gradient, divergence and Laplacian operators are represented at a component-wise level:

$$\nabla_N f = \begin{pmatrix} D_x f \\ D_y f \end{pmatrix}, \quad \nabla_N \cdot \boldsymbol{f} = D_x f^1 + D_y f^2, \quad \Delta_N f = D_x^2 f + D_y^2 f.$$

The following summation by parts formulas are cited from existing studies.

Lemma 2.1 (See [13, 23–25]). (i) *For any $f, g \in \mathcal{M}_h$ and $\boldsymbol{g} \in \mathcal{M}_h \times \mathcal{M}_h$, we have*

$$\langle f, \nabla_N \cdot \boldsymbol{g} \rangle = -\langle \nabla_N f, \boldsymbol{g} \rangle, \quad \langle f, \Delta_N g \rangle = -\langle \nabla_N f, \nabla_N g \rangle = \langle \Delta_N f, g \rangle.$$

(ii) *The inversion of $-\Delta_N$ exists on $\mathcal{M}_h^0$ and $(-\Delta_N)^{-1}$ is self-adjoint and positive definite.*

Since $(-\Delta_N)^{-1} f$ is well-defined for any $f \in \mathcal{M}_h^0$, the discrete H^{-1} inner product and the $\| \cdot \|_{-1,N}$ norm are defined as

$$\langle f, g \rangle_{-1,N} = \langle f, (-\Delta_N)^{-1} g \rangle = \langle (-\Delta_N)^{-1} f, g \rangle, \quad \|f\|_{-1,N} = \sqrt{\langle f, f \rangle_{-1,N}}, \quad \forall\, f, g \in \mathcal{M}_h^0.$$

In terms of the discrete convolution definition, the following kernel function set is considered:

$$\mathcal{K}_h = \{\psi : \Omega_h \to \mathbb{R} \mid \psi_{i+mN_x, j+nN_y} = \psi_{ij} \text{ for any } (i,j) \in S_h \text{ and } (m,n) \in \mathbb{Z}^2\}.$$

A discrete transform and its inverse of $\psi \in \mathcal{K}_h$ can be similarly defined as (2.1) and (2.2). The discrete convolution $\psi \circledast f \in \mathcal{M}_h$ for any $\psi \in \mathcal{K}_h$ and $f \in \mathcal{M}_h$ is defined by

$$(\psi \circledast f)_{ij} = h_x h_y \sum_{(m,n) \in S_h} \psi_{i-m, j-n} f_{mn}, \quad (i,j) \in S_h.$$

The following preliminary estimate is needed in the convergence analysis, and its detailed proof can be found in [23].

Lemma 2.2 (See [23]). *Suppose $\mathsf{J} \in C^1_{\text{per}}(\Omega)$ and denote its grid restriction by $J_{ij} := \mathsf{J}(x_i, y_j)$. Then for any $\phi, \psi \in \mathcal{M}_h$ and any $\alpha > 0$, we have*

$$|\langle J \circledast \phi, \Delta_N \psi \rangle| \leqslant \alpha \|\phi\|_2^2 + \frac{C_2}{\alpha} \|\nabla_N \psi\|_2^2, \tag{2.3}$$

where C_2 is a positive constant that depends on J and Ω, but is independent of h_x and h_y.

Given an integrable kernel J satisfying the assumptions (a)–(e), the discrete form of the nonlocal operator $\mathcal{L}$ becomes

$$\mathcal{L}_N f = (J \circledast 1) f - J \circledast f, \quad f \in \mathcal{M}_h.$$

It is clear that $\mathcal{L}_N$ commutes with $-\Delta_N$ and is self-adjoint and positive semi-definite. On the other hand, a discrete version of the energy (1.2) is defined as

$$E_N(v) = \langle F(v), 1 \rangle + \frac{\varepsilon^2}{2} \langle \mathcal{L}_N v, v \rangle, \quad v \in \mathcal{M}_h.$$

For simplicity, we still use $*$, instead of $\circledast$, to denote the discrete convolutions in the following analysis.

2.2 The stabilized BDF3 discrete scheme

The following third-order accurate in time, stabilized BDF scheme is proposed: given ϕ^n, ϕ^{n-1}, $\phi^{n-2} \in \mathcal{M}_h^0$, find $\phi^{n+1} \in \mathcal{M}_h^0$ that satisfies

$$\begin{aligned} &\frac{\frac{11}{6}\phi^{n+1} - 3\phi^n + \frac{3}{2}\phi^{n-1} - \frac{1}{3}\phi^{n-2}}{\Delta t} \\ &\quad = \Delta_N((\breve{\phi}^{n+1})^3 - A\Delta t \Delta_N(\phi^{n+1} - 2\phi^n + \phi^{n-1}) + \gamma_0 \phi^{n+1} - \varepsilon^2 J * \breve{\phi}^{n+1}) \end{aligned} \tag{2.4}$$

with $\breve{\phi}^{n+1} = 3\phi^n - 3\phi^{n-1} + \phi^{n-2}$.

Of course, the unique solvability of this numerical method is obvious, based on the fact that only a linear and positive-definite operator, i.e., $\frac{11}{6\Delta t} - \gamma_0 \Delta_N + A\Delta t \Delta_N^2$, is involved in the implicit part. In fact, the spatial interpolation of the Fourier basis functions forms a complete basis of all the eigenvectors of this linear operator, and all the eigenvalues can be exactly computed. In turn, such a linear system can be exactly solved via a fast Fourier transform-based implementation, which turns out to be highly efficient.

2.3 A modified energy stability analysis

A modified energy stability estimate is stated in the following proposition.

Proposition 2.3. *For the proposed BDF3 numerical scheme* (2.4)*, a modified energy dissipation property holds*:

$$\tilde{E}_N(\phi^{n+1},\phi^n,\phi^{n-1}) \leqslant \tilde{E}_N(\phi^n,\phi^{n-1},\phi^{n-2}), \tag{2.5}$$

where

$$\begin{aligned}\tilde{E}_N(\phi^{n+1},\phi^n,\phi^{n-1}) :=& E_N(\phi^{n+1}) + \frac{3}{4\Delta t}\|\phi^{n+1}-\phi^n\|_{-1,N}^2 + \frac{1}{6\Delta t}\|\phi^n-\phi^{n-1}\|_{-1,N}^2 \\ &+ \left(\frac{7}{24}A\right)^{\frac{1}{2}}\|\phi^{n+1}-2\phi^n+\phi^{n-1}\|_2^2 + \frac{A\Delta t}{2}\|\nabla_N(\phi^{n+1}-\phi^n)\|_2^2,\end{aligned}$$

provided that the following constraints are valid:

$$A \geqslant \frac{24}{7}\left(\frac{9}{2\gamma_0}(\|3\phi^n-3\phi^{n-1}+\phi^{n-2}\|_\infty^2+\|\phi^{n+1}\|_\infty^2)^4+1\right)^2, \quad 24C_2\varepsilon^4\Delta t \leqslant \min(1,\gamma_0). \tag{2.6}$$

Proof. Taking a discrete inner product with (2.4) by $(-\Delta_N)^{-1}(\phi^{n+1}-\phi^n)$ leads to

$$\begin{aligned}&\frac{1}{\Delta t}\left\langle \frac{11}{6}\phi^{n+1}-3\phi^n+\frac{3}{2}\phi^{n-1}-\frac{1}{3}\phi^{n-2}, \phi^{n+1}-\phi^n\right\rangle_{-1,N} \\ &\quad - A\Delta t\langle \Delta_N(\phi^{n+1}-2\phi^n+\phi^{n-1}), \phi^{n+1}-\phi^n\rangle + \gamma_0\langle \phi^{n+1},\phi^{n+1}-\phi^n\rangle \\ &\quad = -\langle (\breve{\phi}^{n+1})^3, \phi^{n+1}-\phi^n\rangle + \varepsilon^2\langle J*\breve{\phi}^{n+1}, \phi^{n+1}-\phi^n\rangle,\end{aligned} \tag{2.7}$$

in which summation by parts formulas have been repeatedly applied. For the left-hand side term associated with the BDF3 temporal stencil, we make use of the following equivalent form:

$$\begin{aligned}&\frac{11}{6}\phi^{n+1}-3\phi^n+\frac{3}{2}\phi^{n-1}-\frac{1}{3}\phi^{n-2} \\ &\quad = \frac{2}{3}(\phi^{n+1}-\phi^n)+\frac{7}{6}(\phi^{n+1}-2\phi^n+\phi^{n-1})+\frac{1}{3}(\phi^{n-1}-\phi^{n-2}).\end{aligned}$$

This in turn gives the following estimate:

$$\begin{aligned}&\left\langle \frac{11}{6}\phi^{n+1}-3\phi^n+\frac{3}{2}\phi^{n-1}-\frac{1}{3}\phi^{n-2}, \phi^{n+1}-\phi^n\right\rangle_{-1,N} \\ &\quad \geqslant \frac{2}{3}\|\phi^{n+1}-\phi^n\|_{-1,N}^2 - \frac{1}{6}\|\phi^{n+1}-\phi^n\|_{-1,N}^2 - \frac{1}{6}\|\phi^{n-1}-\phi^{n-2}\|_{-1,N}^2 \\ &\qquad + \frac{7}{12}(\|\phi^{n+1}-\phi^n\|_{-1,N}^2 - \|\phi^n-\phi^{n-1}\|_{-1,N}^2 + \|\phi^{n+1}-2\phi^n+\phi^{n-1}\|_{-1,N}^2) \\ &\quad = \frac{13}{12}\|\phi^{n+1}-\phi^n\|_{-1,N}^2 - \frac{7}{12}\|\phi^n-\phi^{n-1}\|_{-1,N}^2 - \frac{1}{6}\|\phi^{n-1}-\phi^{n-2}\|_{-1,N}^2 \\ &\qquad + \frac{7}{12}\|\phi^{n+1}-2\phi^n+\phi^{n-1}\|_{-1,N}^2.\end{aligned} \tag{2.8}$$

For the artificial regularization term, the following identity holds:

$$\begin{aligned}&\langle -\Delta_N(\phi^{n+1}-2\phi^n+\phi^{n-1}), \phi^{n+1}-\phi^n\rangle \\ &\quad = \langle \nabla_N(\phi^{n+1}-2\phi^n+\phi^{n-1}), \nabla_N(\phi^{n+1}-\phi^n)\rangle \\ &\quad = \frac{1}{2}(\|\nabla_N(\phi^{n+1}-\phi^n)\|_2^2 - \|\nabla_N(\phi^n-\phi^{n-1})\|_2^2 + \|\nabla_N(\phi^{n+1}-2\phi^n+\phi^{n-1})\|_2^2).\end{aligned} \tag{2.9}$$

The standard triangular equality can be applied to the linear term on the left-hand side

$$\langle \phi^{n+1}, \phi^{n+1}-\phi^n\rangle = \frac{1}{2}(\|\phi^{n+1}\|_2^2 - \|\phi^n\|_2^2 + \|\phi^{n+1}-\phi^n\|_2^2). \tag{2.10}$$

Regarding the nonlocal diffusion term on the right-hand side, we begin with a rewritten form

$$\begin{aligned}-\varepsilon^2\langle J*\breve{\phi}^{n+1},\phi^{n+1}-\phi^n\rangle &= -\varepsilon^2\langle J*\phi^{n+1},\phi^{n+1}-\phi^n\rangle\\ &\quad+\varepsilon^2\langle J*(\phi^{n+1}-3\phi^n+3\phi^{n-1}-\phi^{n-2}),\phi^{n+1}-\phi^n\rangle\\ &= -\frac{\varepsilon^2}{2}(\langle\phi^{n+1},J*\phi^{n+1}\rangle-\langle\phi^n,J*\phi^n\rangle+\langle J*(\phi^{n+1}-\phi^n),\phi^{n+1}-\phi^n\rangle)\\ &\quad+\varepsilon^2\langle J*(\phi^{n+1}-3\phi^n+3\phi^{n-1}-\phi^{n-2}),\phi^{n+1}-\phi^n\rangle. \end{aligned}\tag{2.11}$$

For the additional term $\varepsilon^2\langle J*(\phi^{n+1}-\phi^n),\phi^{n+1}-\phi^n\rangle$, we apply (2.3) in Lemma 2.2 and get

$$\begin{aligned}&\varepsilon^2\langle J*(\phi^{n+1}-\phi^n),\phi^{n+1}-\phi^n\rangle\\ &\quad=-\varepsilon^2\langle J*(\phi^{n+1}-\phi^n),\Delta_N((-\Delta_N)^{-1}(\phi^{n+1}-\phi^n))\rangle\\ &\quad\leqslant 6C_2\varepsilon^4\Delta t\|\phi^{n+1}-\phi^n\|_2^2+\frac{1}{6\Delta t}\|\nabla_N(-\Delta_N)^{-1}(\phi^{n+1}-\phi^n)\|_2^2\\ &\quad\leqslant 6C_2\varepsilon^4\Delta t\|\phi^{n+1}-\phi^n\|_2^2+\frac{1}{6\Delta t}\|\phi^{n+1}-\phi^n\|_{-1,N}^2. \end{aligned}\tag{2.12}$$

Another additional term, $\varepsilon^2\langle J*(\phi^{n+1}-3\phi^n+3\phi^{n-1}-\phi^{n-2}),\phi^{n+1}-\phi^n\rangle$, can be analyzed in a similar way:

$$\begin{aligned}&\varepsilon^2\langle J*(\phi^{n+1}-3\phi^n+3\phi^{n-1}-\phi^{n-2}),\phi^{n+1}-\phi^n\rangle\\ &\quad=-\varepsilon^2\langle J*(\phi^{n+1}-3\phi^n+3\phi^{n-1}-\phi^{n-2}),\Delta_N((-\Delta_N)^{-1}(\phi^{n+1}-\phi^n))\rangle\\ &\quad\geqslant -12C_2\varepsilon^4\Delta t\|\phi^{n+1}-3\phi^n+3\phi^{n-1}-\phi^{n-2}\|_2^2-\frac{1}{12\Delta t}\|\phi^{n+1}-\phi^n\|_{-1,N}^2\\ &\quad\geqslant -24C_2\varepsilon^4\Delta t(\|\phi^{n+1}-2\phi^n+\phi^{n-1}\|_2^2+\|\phi^n-2\phi^{n-1}+\phi^{n-2}\|_2^2)-\frac{1}{12\Delta t}\|\phi^{n+1}-\phi^n\|_{-1,N}^2. \end{aligned}\tag{2.13}$$

As a result, a combination of (2.11)–(2.13) yields

$$\begin{aligned}&-\varepsilon^2\langle J*\breve{\phi}^{n+1},\phi^{n+1}-\phi^n\rangle\\ &\quad\geqslant-\frac{\varepsilon^2}{2}(\langle\phi^{n+1},J*\phi^{n+1}\rangle-\langle\phi^n,J*\phi^n\rangle)-\frac{1}{6\Delta t}\|\phi^{n+1}-\phi^n\|_{-1,N}^2\\ &\qquad-C_2\varepsilon^4\Delta t(3\|\phi^{n+1}-\phi^n\|_2^2+24\|\phi^{n+1}-2\phi^n+\phi^{n-1}\|_2^2+24\|\phi^n-2\phi^{n-1}+\phi^{n-2}\|_2^2). \end{aligned}\tag{2.14}$$

In terms of the nonlinear inner product, we begin with the following decomposition:

$$(\breve{\phi}^{n+1})^3-(\phi^{n+1})^3=-((\breve{\phi}^{n+1})^2+\breve{\phi}^{n+1}\phi^{n+1}+(\phi^{n+1})^2)(\phi^{n+1}-3\phi^n+3\phi^{n-1}-\phi^{n-2}),\tag{2.15}$$

where the identity $\breve{\phi}^{n+1}-\phi^{n+1}=-(\phi^{n+1}-3\phi^n+3\phi^{n-1}-\phi^{n-2})$ has been applied. In turn, the following estimate can be derived:

$$\begin{aligned}&\langle(\breve{\phi}^{n+1})^3-(\phi^{n+1})^3,\phi^{n+1}-\phi^n\rangle\\ &\quad\geqslant\|(\breve{\phi}^{n+1})^2+\breve{\phi}^{n+1}\phi^{n+1}+(\phi^{n+1})^2\|_\infty\cdot\|\phi^{n+1}-3\phi^n+3\phi^{n-1}-\phi^{n-2}\|_2\cdot\|\phi^{n+1}-\phi^n\|_2\\ &\quad\geqslant-\frac{3}{2}(\|\breve{\phi}^{n+1}\|_\infty^2+\|\phi^{n+1}\|_\infty^2)\cdot\|\phi^{n+1}-3\phi^n+3\phi^{n-1}-\phi^{n-2}\|_2\cdot\|\phi^{n+1}-\phi^n\|_2\\ &\quad\geqslant-\frac{9}{4\gamma_0}(\|\breve{\phi}^{n+1}\|_\infty^2+\|\phi^{n+1}\|_\infty^2)^2\|\phi^{n+1}-3\phi^n+3\phi^{n-1}-\phi^{n-2}\|_2^2-\frac{\gamma_0}{4}\|\phi^{n+1}-\phi^n\|_2^2\\ &\quad\geqslant-\frac{9}{2\gamma_0}(\|\breve{\phi}^{n+1}\|_\infty^2+\|\phi^{n+1}\|_\infty^2)^2(\|\phi^{n+1}-2\phi^n+\phi^{n-1}\|_2^2+\|\phi^n-2\phi^{n-1}+\phi^{n-2}\|_2^2)\\ &\qquad-\frac{\gamma_0}{4}\|\phi^{n+1}-\phi^n\|_2^2. \end{aligned}\tag{2.16}$$

On the other hand, the convexity of $\|\phi\|_4^4$ (in terms of ϕ) implies the following inequality:

$$\langle(\phi^{n+1})^3,\phi^{n+1}-\phi^n\rangle\geqslant\frac{1}{4}(\|\phi^{n+1}\|_4^4-\|\phi^n\|_4^4),\tag{2.17}$$

and its combination with (2.16) leads to

$$\begin{aligned}\langle(\breve{\phi}^{n+1})^3, \phi^{n+1}-\phi^n\rangle \geqslant & \frac{1}{4}(\|\phi^{n+1}\|_4^4-\|\phi^n\|_4^4)-\frac{\gamma_0}{4}\|\phi^{n+1}-\phi^n\|_2^2\\ & -\frac{9}{2\gamma_0}(\|\breve{\phi}^{n+1}\|_\infty^2+\|\phi^{n+1}\|_\infty^2)^2(\|\phi^{n+1}-2\phi^n+\phi^{n-1}\|_2^2\\ & +\|\phi^n-2\phi^{n-1}+\phi^{n-2}\|_2^2). \end{aligned} \tag{2.18}$$

Finally, a substitution of (2.8)–(2.10), (2.14) and (2.18) into (2.7) yields

$$\begin{aligned}&\frac{1}{\Delta t}\left(\frac{11}{12}\|\phi^{n+1}-\phi^n\|_{-1,N}^2-\frac{7}{12}\|\phi^n-\phi^{n-1}\|_{-1,N}^2-\frac{1}{6}\|\phi^{n-1}-\phi^{n-2}\|_{-1,N}^2\right)\\ &\quad+E_N(\phi^{n+1})-E_N(\phi^n)+\frac{A\Delta t}{2}(\|\nabla_N(\phi^{n+1}-\phi^n)\|_2^2-\|\nabla_N(\phi^n-\phi^{n-1})\|_2^2)\\ &\quad+\frac{7}{12\Delta t}\|\phi^{n+1}-2\phi^n+\phi^{n-1}\|_{-1,N}^2+\frac{A\Delta t}{2}\|\nabla_N(\phi^{n+1}-2\phi^n+\phi^{n-1})\|_2^2\\ &\quad-\left(\frac{9}{2\gamma_0}(\|\breve{\phi}^{n+1}\|_\infty^2+\|\phi^{n+1}\|_\infty^2)^2+24C_2\varepsilon^4\Delta t\right)\cdot(\|\phi^{n+1}-2\phi^n+\phi^{n-1}\|_2^2+\|\phi^n-2\phi^{n-1}+\phi^{n-2}\|_2^2)\\ &\quad+\left(\frac{\gamma_0}{4}-3C_2\varepsilon^4\Delta t\right)\|\phi^{n+1}-\phi^n\|_2^2\leqslant 0. \end{aligned} \tag{2.19}$$

Meanwhile, a careful application of the Cauchy inequality indicates that

$$\begin{aligned}&\frac{7}{12\Delta t}\|\phi^{n+1}-2\phi^n+\phi^{n-1}\|_{-1,N}^2+\frac{A\Delta t}{2}\|\nabla_N(\phi^{n+1}-2\phi^n+\phi^{n-1})\|_2^2\\ &\quad\geqslant\left(\frac{7}{6}A\right)^{\frac{1}{2}}\|\phi^{n+1}-2\phi^n+\phi^{n-1}\|_2^2. \end{aligned} \tag{2.20}$$

In turn, its substitution into (2.19) leads to a modified energy dissipation

$$\tilde{E}_N(\phi^{n+1},\phi^n,\phi^{n-1})-\tilde{E}_N(\phi^n,\phi^{n-1},\phi^{n-2})+\frac{1}{6\Delta t}\|\phi^{n+1}-\phi^n\|_{-1,N}^2+\frac{\gamma_0}{8}\|\phi^{n+1}-\phi^n\|_2^2\leqslant 0 \tag{2.21}$$

under the constraint (2.6), to which the following bounds have been applied:

$$\begin{aligned}&24C_2\varepsilon^4\Delta t\leqslant 1,\quad 3C_2\varepsilon^4\Delta t\leqslant\frac{\gamma_0}{8},\\ &\frac{9}{2\gamma_0}(\|\breve{\phi}^{n+1}\|_\infty^2+\|\phi^{n+1}\|_\infty^2)^2+1\leqslant\left(\frac{7}{24}A\right)^{\frac{1}{2}}=\frac{1}{2}\left(\frac{7}{6}A\right)^{\frac{1}{2}}. \end{aligned}$$

This completes the proof of Proposition 2.3. □

Remark 2.4. There have been a few existing studies of the BDF3 schemes for various gradient flows with the standard local diffusion process [8, 17], and the associated energy stability and convergence analysis have been reported as well. Meanwhile, it is noticed that an implicit treatment for the nonlinear term is adopted in [8] to deal with the standard local Cahn-Hilliard equation, so that the artificial regularization parameter requirement turns out to be simpler than (2.6) stated in Proposition 2.3. In addition, the theoretical analysis for the NCH equation is much more challenging than that for the local gradient flows, which comes from the lack of diffusion regularity in the nonlocal model.

Remark 2.5. It is natural to inquire about an extension of this framework to even higher-order methods, such as the BDF4. While higher-order accuracy can be achieved via multi-step formulas, such as the exponential time differencing (ETD) schemes for the no-slope-selection model in [7], extending the current BDF theoretical analysis would face fundamental challenges. Specifically, the energy stability analysis for higher-order multi-step schemes consistently relies on a modified energy functional. In terms of the BDF4 algorithm, although it is G-stable, constructing such a modified energy functional to absorb the explicit extrapolation of the nonlinear term turns out to be algebraically complex, as the

decomposition identity becomes significantly more complicated. Furthermore, the stability region of the BDF4 is narrower than that of the BDF3, which would likely necessitate a much larger stabilization parameter A or stricter time-step constraint to enforce the modified energy dissipation.

Remark 2.6. As always in the stabilization numerical analysis, the constraint (2.6) depends on the maximum norm bound of the numerical solution at the next time step, as well as those at the current and previous time steps. Meanwhile, a direct $\|\cdot\|_\infty$ estimate of the numerical solution is not theoretically available, so this proposition does not provide a closed mathematical analysis of the energy stability. As a result, the maximum norm bound of the numerical solution has to be derived to recover such a theoretical analysis. For the standard local Cahn-Hilliard equation, the $\|\cdot\|_\infty$ bound of the numerical solution can be justified in the usual Sobolev space, with the help of the standard local diffusion operator; see the related studies [19–21]. On the other hand, since the nonlocal diffusion operator with an integrable kernel generally acts as a bounded linear operator and lacks the strong regularity to facilitate Sobolev embeddings, a direct $\|\cdot\|_\infty$ estimate would not be available for the NCH equation. Instead, the convergence analysis turns out to be necessary to recover such a maximum norm bound. It should be noted that the lower bound for A in (2.6) serves as a theoretical sufficiency condition and may be conservative in practice. As shown in Subsection 4.1, the scheme performs robustly with much smaller values of A, suggesting that a sharper practical bound exists.

In other words, the lower bound of A has to be obtained by deriving the maximum bound of the numerical solution at the specified time steps. To deal with this challenge, a perturbation analysis turns to be a more feasible approach. In more detail, the numerical solution has to be treated as a perturbation of the exact PDE solution for (1.3), and a local-in-time convergence analysis is performed to recover the maximum norm bound of the numerical solution, with the help of the inverse inequality.

3 The optimal rate convergence analysis and error estimate

A smooth, periodic solution to the NCH equation (1.3), with smooth periodic initial data, is denoted by Φ.

On the other hand, since the NCH equation (1.3) is a mass-conservative gradient flow, we need to construct a mean-free numerical error function to facilitate the H^{-1} error analysis. To accomplish this, we introduce $\Phi_N(\cdot\,,t) := \mathcal{P}_N\Phi(\cdot\,,t)$, the (spatial) Fourier projection of the exact solution into $\mathcal{B}^K$, the space of trigonometric polynomials of degree up to K, with $K = [\frac{N}{2}]$. Subsequently, the following projection approximation becomes standard:

$$\|\Phi_N - \Phi\|_{L^\infty(0,T;H^k)} \leqslant Ch^{\ell-k}\|\Phi\|_{L^\infty(0,T;H^\ell)}, \quad \forall\, 0 \leqslant k \leqslant \ell,$$

if $\Phi \in L^\infty(0,T;H^\ell_{\rm per}(\Omega))$, for some $\ell \in \mathbb{N}$. For simplicity of notation, we define Φ_N^k and Φ^k as $\Phi_N(\cdot\,,t_k)$ and $\Phi(\cdot\,,t_k)$, respectively, with $t_k = k\cdot\Delta t$. Based on the fact that $\Phi_N \in \mathcal{B}^K$, the mass conservative property is valid at the discrete level:

$$\overline{\Phi_N^k} = \frac{1}{|\Omega|}\int_\Omega \Phi_N(\cdot,t_k)\,d\boldsymbol{x} = \frac{1}{|\Omega|}\int_\Omega \Phi_N(\cdot,t_{k-1})\,d\boldsymbol{x} = \overline{\Phi_N^{k-1}}, \quad \forall\, k\in\mathbb{N}.$$

Meanwhile, the solution of the numerical scheme (2.4) is also mass conservative at the discrete level:

$$\overline{\phi^k} = \overline{\phi^{k-1}}, \quad \forall\, k\in\mathbb{N}.$$

On the other hand, we define Φ_N^k as the interpolation values of Φ_N at discrete grid points at time instant t^k: $\Phi_N^k := \mathcal{P}_h\Phi_N(\cdot\,,t^k)$. To avoid an initial inconsistency, we use the mass conservative projection for the initial data: $\phi^0_{i,j,k} := \Phi_N(x_i,y_j,z_k,t=0)$. In turn, the error grid function is defined as

$$e^k := \Phi_N^k - \phi^k, \quad \forall\, k \geqslant 0.$$

Consequently, it is clear that $\overline{e^k} = 0$ for any $k \geqslant 0$, so that the discrete norm $\|\cdot\|_{-1,N}$ is well-defined for the error grid function. In addition, with an initial data with sufficient regularity, we are always able to assume that the exact solution has regularity of class $\mathcal{R}$:

$$\Phi \in \mathcal{R} := H^4(0,T;C^0_{\rm per}) \cap H^3(0,T;C^2_{\rm per}) \cap L^\infty(0,T;C^{m+2}_{\rm per}), \quad m \geqslant 3. \tag{3.1}$$

Here, the integer m denotes the spatial regularity index of the exact solution. As a result, the following functional bound becomes valid:

$$\max_{1\leqslant j\leqslant N_k} \|\Phi_N^j\|_\infty + \max_{1\leqslant j\leqslant N_k} \left\| \frac{\Phi_N^j - \Phi_N^{j-1}}{\Delta t} \right\|_\infty + \max_{1\leqslant j\leqslant N_k} \left\| \frac{\Phi_N^{j+1} - 2\Phi_N^j + \Phi_N^{j-1}}{\Delta t^2} \right\|_\infty < C^*, \tag{3.2}$$

which states that the exact solution, as well as its first- and second-order temporal derivatives, stays bounded in both time and space.

Theorem 3.1. *Given smooth, periodic initial data $\Phi(x,y,z,t=0)$, suppose the unique, smooth, periodic solution for the NCH equation* (1.3) *is given by $\Phi(x,y,t)$ on Ω for $0 < t \leqslant T$, for some $T < \infty$. In addition, the following assumption is made for the constant A:*

$$\begin{aligned} &A \geqslant \frac{24}{7}\left(\frac{18M_0^4}{\gamma_0} + 1\right)^2, \quad \text{with } M_0 = 1 + C^*, \\ &C^* = \max_{1\leqslant j\leqslant N_k} (\|\Phi_N^j\|_\infty + \|\partial_t \Phi_N^j\|_\infty + \|\partial_t^2 \Phi_N^j\|_\infty) \end{aligned} \tag{3.3}$$

under a mild time step constraint $24C_2\varepsilon^4\Delta t \leqslant 1$. Then, provided that Δt and h are sufficiently small, under a linear refinement path constraint $C_1 h \leqslant \Delta t \leqslant C_2 h$, with C being any fixed constant, we have

$$\|e^n\|_2 \leqslant C(\Delta t^3 + h^m), \quad m \geqslant 3 \tag{3.4}$$

for all positive integers n, such that $n\,\Delta t \leqslant T$, where m corresponds to the spatial regularity index defined in (3.1)*, and $C > 0$ is independent of h and Δt.*

Because of the third-order temporal accuracy, combined with the spectral accuracy in the spatial approximation, a higher-order consistency analysis is not needed for this numerical scheme. In fact, a direct substitution of the Fourier projection solution Φ_N into the numerical system reveals an $(\Delta t^3 + h^m)$ accuracy:

$$\begin{aligned} &\frac{\frac{11}{6}\Phi_N^{n+1} - 3\Phi_N^n + \frac{3}{2}\Phi_N^{n-1} - \frac{1}{3}\Phi_N^{n-2}}{\Delta t} \\ &\quad = \Delta_N((\breve{\Phi}_N^{n+1})^3 + \gamma_0\Phi_N^{n+1} - A\Delta t\Delta_N(\Phi_N^{n+1} - 2\Phi_N^n + \Phi_N^{n-1}) - \varepsilon^2 J * \breve{\Phi}_N^{n+1}) + \tau_0^{n+1} \end{aligned} \tag{3.5}$$

with

$$\breve{\Phi}_N^{n+1} = 3\Phi_N^n - 3\Phi_N^{n-1} + \Phi_N^{n-2}, \quad \|\tau_0^{n+1}\|_{-1,N} \leqslant C(\Delta t^3 + h^m).$$

Moreover, by the regularity assumption (3.2) for the exact projection solution Φ_N, we are able to obtain the following functional bounds, which are needed in the later convergence analysis:

$$\|\Phi_N^{j+1} - \Phi_N^j\|_\infty \leqslant C^*\Delta t, \quad \|\Phi_N^{j+1} - 2\Phi_N^j + \Phi_N^{j-1}\|_\infty \leqslant C^*\Delta t^2, \quad n-2 \leqslant j \leqslant n, \tag{3.6}$$

together with

$$\begin{aligned} \|\breve{\Phi}_N^{n+1}\|_\infty &= \|\Phi_N^n + 2(\Phi_N^n - \Phi_N^{n-1}) - (\Phi_N^{n-1} - \Phi_N^{n-2})\|_\infty \\ &\leqslant \|\Phi_N^n\|_\infty + 2\|\Phi_N^n - \Phi_N^{n-1}\|_\infty + \|\Phi_N^{n-1} - \Phi_N^{n-2}\|_\infty \\ &\leqslant C^* + 3C^*\Delta t \leqslant C^* + \frac{1}{2} \leqslant M_0 \end{aligned} \tag{3.7}$$

and

$$\|\Phi_N^{n+1} - \breve{\Phi}_N^{n+1}\|_\infty = \|(\Phi_N^{n+1} - 2\Phi_N^n + \Phi_N^{n-1}) - (\Phi_N^n - 2\Phi_N^{n-1} + \Phi_N^{n-2})\|_\infty$$

$$\leqslant \|\Phi_N^{n+1} - 2\Phi_N^n + \Phi_N^{n-1}\|_\infty + \|\Phi_N^n - 2\Phi_N^{n-1} + \Phi_N^{n-2}\|_\infty$$
$$\leqslant 2C^*\Delta t^2 \leqslant \frac{1}{4}\Delta t, \tag{3.8}$$

provided that Δt is sufficiently small.

Subsequently, subtracting (2.4) from (3.5) yields

$$\frac{\frac{11}{6}e^{n+1} - 3e^n + \frac{3}{2}e^{n-1} + \frac{1}{3}e^{n-2}}{\Delta t} = \Delta_N((\breve{\Phi}_N^{n+1})^3 - (\breve{\phi}^{n+1})^3 + \gamma_0 e^{n+1} - \varepsilon^2 J * \breve{e}^{n+1}$$
$$- A\Delta t\Delta_N(e^{n+1} - 2e^n + e^{n-1})) + \tau_0^{n+1}, \tag{3.9}$$
$$\breve{e}^{n+1} := 3e^n - 3e^{n-1} + e^{n-2}. \tag{3.10}$$

To carry out the nonlinear error estimate, we make an $\|\cdot\|_2$ assumption for the numerical error function at the previous time steps t^n, t^{n-1} and t^{n-2}:

$$\|e^k\|_2 \leqslant \Delta t^{\frac{11}{4}} + h^{m-1}, \quad k = n, n-1, n-2. \tag{3.11}$$

Remark 3.2. Since the BDF3 is a multi-step scheme, the numerical solutions at the first two steps ϕ^1 and ϕ^2 are required to initialize the induction. In this analysis, we assume that these starting values are computed by a sufficiently accurate one-step method (e.g., the classical fourth-order Runge-Kutta method), so that the error bounds in (3.11) are satisfied for the base cases $k = 0, 1, 2$. Using a high-order initialization ensures that the starting error remains $O(\Delta t^3)$, consistent with the global temporal accuracy order.

In turn, an application of the inverse inequality implies that

$$\|e^k\|_\infty \leqslant \frac{C\|\hat{e}^k\|_2}{h^{\frac{3}{2}}} \leqslant C(\Delta t^{\frac{5}{4}} + h^{m-\frac{5}{2}}) \leqslant \frac{1}{8}\Delta t, \quad k = n, n-1, n-2,$$

so that

$$\|\breve{e}^{n+1}\|_\infty = \|3e^n - 3e^{n-1} + e^{n-2}\|_\infty \leqslant 3\|e^n\|_\infty + 3\|e^{n-1}\|_\infty + \|e^{n-2}\|_\infty \leqslant \frac{7}{8}\Delta t \leqslant \Delta t \tag{3.12}$$

under the linear refinement constraint $C_1 h \leqslant \Delta t \leqslant C_2 h$. In turn, $\|\cdot\|_\infty$ bound for the numerical solutions at the previous time steps becomes available

$$\|\phi^k\|_\infty = \|\Phi_N^k - e^k\|_\infty \leqslant \|\Phi_N^k\|_\infty + \|e^k\|_\infty \leqslant C^* + \frac{1}{8}\Delta t \leqslant M_0, \quad k = n, n-1, n-2,$$
$$\|\breve{\phi}^{n+1}\|_\infty = \|\breve{\Phi}_N^{n+1} - \breve{e}^{n+1}\|_\infty \leqslant \|\breve{\Phi}_N^{n+1}\|_\infty + \|\breve{e}^{n+1}\|_\infty \leqslant C^* + \frac{1}{2} + \frac{7}{8}\Delta t \leqslant C^* + 1 = M_0, \tag{3.13}$$

in which the bound (3.7) (for Φ_N) has been applied. In fact, the *a priori* assumption (3.11) is recovered in the convergence estimate, as will be demonstrated later.

Since $\overline{e^k} = 0$ for any $k \geqslant 0$, $(-\Delta_N)^{-1}e^k$ has been well-defined. Taking a discrete inner product with (3.9) by $(-\Delta_N)^{-1}(e^{n+1} - e^n)$ leads to

$$\frac{1}{\Delta t}\left\langle \frac{11}{6}e^{n+1} - 3e^n + \frac{3}{2}e^{n-1} - \frac{1}{3}e^{n-2}, e^{n+1} - e^n \right\rangle_{-1,N} + \gamma_0\langle e^{n+1}, e^{n+1} - e^n\rangle$$
$$- A\Delta t\langle \Delta_N(e^{n+1} - 2e^n + e^{n-1}), e^{n+1} - e^n\rangle - \varepsilon^2\langle J * \breve{e}^{n+1}, e^{n+1} - e^n\rangle$$
$$= -\langle(\breve{\Phi}_N^{n+1})^3 - (\breve{\phi}^{n+1})^3, e^{n+1} - e^n\rangle + \Delta t\langle(-\Delta_N)^{-1}(e^{n+1} - e^n), \tau_0^{n+1}\rangle, \tag{3.14}$$

in which summation by parts formulas have been repeatedly applied. The left-hand side terms can be analyzed in a similar fashion as in (2.8)–(2.10), as well as (2.11)–(2.14):

$$\left\langle \frac{11}{6}e^{n+1} - 3e^n + \frac{3}{2}e^{n-1} - \frac{1}{3}e^{n-2}, e^{n+1} - e^n \right\rangle_{-1,N}$$

$$\geqslant \frac{13}{12}\|e^{n+1}-e^n\|_{-1,N}^2-\frac{7}{12}\|e^n-e^{n-1}\|_{-1,N}^2-\frac{1}{6}\|e^{n-1}-e^{n-2}\|_{-1,N}^2$$
$$+\frac{7}{12}\|e^{n+1}-2e^n+e^{n-1}\|_{-1,N}^2, \tag{3.15}$$

$$\langle-\Delta_N(e^{n+1}-2e^n+e^{n-1}),e^{n+1}-e^n\rangle$$
$$=\frac{1}{2}(\|\nabla_N(e^{n+1}-e^n)\|_2^2-\|\nabla_N(e^n-e^{n-1})\|_2^2+\|\nabla_N(e^{n+1}-2e^n+e^{n-1})\|_2^2) \tag{3.16}$$

and

$$\langle e^{n+1},e^{n+1}-e^n\rangle=\frac{1}{2}(\|e^{n+1}\|_2^2-\|e^n\|_2^2+\|e^{n+1}-e^n\|_2^2). \tag{3.17}$$

The last term on the left-hand side of (3.14) can be decomposed into the following two parts:

$$-\varepsilon^2\langle J*\breve{e}^{n+1},e^{n+1}-e^n\rangle=-\varepsilon^2\langle J*e^{n+1},e^{n+1}-e^n\rangle$$
$$+\varepsilon^2\langle J*(e^{n+1}-3e^n+3e^{n-1}-e^{n-2}),e^{n+1}-e^n\rangle. \tag{3.18}$$

Thus, the first term can be bounded as

$$\varepsilon^2\langle J*e^{n+1},e^{n+1}-e^n\rangle=-\varepsilon^2\langle J*e^{n+1},\Delta_N((-\Delta_N)^{-1}(e^{n+1}-e^n))\rangle$$
$$\leqslant 12C_2\varepsilon^4\Delta t\|e^{n+1}\|_2^2+\frac{1}{12\Delta t}\|e^{n+1}-e^n\|_{-1,N}^2, \tag{3.19}$$

and the second term is estimated as

$$\varepsilon^2\langle J*(e^{n+1}-3e^n+3e^{n-1}-e^{n-2}),e^{n+1}-e^n\rangle$$
$$\geqslant -12C_2\varepsilon^4\Delta t\|e^{n+1}-3e^n+3e^{n-1}-e^{n-2}\|_2^2-\frac{1}{12\Delta t}\|e^{n+1}-e^n\|_{-1,N}^2$$
$$\geqslant -24C_2\varepsilon^4\Delta t(\|e^{n+1}-2e^n+e^{n-1}\|_2^2+\|e^n-2e^{n-1}+e^{n-2}\|_2^2)-\frac{1}{12\Delta t}\|e^{n+1}-e^n\|_{-1,N}^2, \tag{3.20}$$

we then have

$$-\varepsilon^2\langle J*\breve{e}^{n+1},e^{n+1}-e^n\rangle$$
$$\geqslant -12C_2\varepsilon^4\Delta t\|e^{n+1}\|_2^2-\frac{1}{6\Delta t}\|\phi^{n+1}-\phi^n\|_{-1,N}^2$$
$$-24C_2\varepsilon^4\Delta t(\|\phi^{n+1}-2\phi^n+\phi^{n-1}\|_2^2+\|\phi^n-2\phi^{n-1}+\phi^{n-2}\|_2^2). \tag{3.21}$$

For the nonlinear inner product on the right-hand side of (3.14), we begin with the following nonlinear expansion:

$$(\breve{\Phi}_N^{n+1})^3-(\breve{\phi}^{n+1})^3=((\breve{\Phi}_N^{n+1})^2+\breve{\Phi}_N^{n+1}\breve{\phi}^{n+1}+(\breve{\phi}^{n+1})^2)\breve{e}^{n+1}$$
$$=((\breve{\Phi}_N^{n+1})^2+\breve{\Phi}_N^{n+1}\breve{\phi}^{n+1}+(\breve{\phi}^{n+1})^2)e^{n+1}$$
$$-((\breve{\Phi}_N^{n+1})^2+\breve{\Phi}_N^{n+1}\breve{\phi}^{n+1}+(\breve{\phi}^{n+1})^2)(e^{n+1}-3e^n+3e^{n-1}-e^{n-2}). \tag{3.22}$$

In terms of the second expansion part, its inner product with $e^{n+1}-e^n$ has the following upper bound:

$$\langle((\breve{\Phi}_N^{n+1})^2+\breve{\Phi}_N^{n+1}\breve{\phi}^{n+1}+(\breve{\phi}^{n+1})^2)(e^{n+1}-3e^n+3e^{n-1}-e^{n-2}),e^{n+1}-e^n\rangle$$
$$\leqslant\|(\breve{\Phi}_N^{n+1})^2+\breve{\Phi}_N^{n+1}\breve{\phi}^{n+1}+(\breve{\phi}^{n+1})^2\|_\infty\cdot\|e^{n+1}-3e^n+3e^{n-1}-e^{n-2}\|_2\cdot\|e^{n+1}-e^n\|_2$$
$$\leqslant 3M_0^2\|e^{n+1}-3e^n+3e^{n-1}-e^{n-2}\|_2\cdot\|e^{n+1}-e^n\|_2$$
$$\leqslant\frac{9M_0^4}{\gamma_0}\|e^{n+1}-3e^n+3e^{n-1}-e^{n-2}\|_2^2+\frac{\gamma_0}{4}\|e^{n+1}-e^n\|_2^2$$
$$\leqslant\frac{18M_0^4}{\gamma_0}(\|e^{n+1}-2e^n+e^{n-1}\|_2^2+\|e^n-2e^{n-1}+e^{n-2}\|_2^2)+\frac{\gamma_0}{4}\|e^{n+1}-e^n\|_2^2, \tag{3.23}$$

in which the following $\|\cdot\|_\infty$ bound has been applied, which comes from a combination of the preliminary bound (3.7) and the *a priori* estimate (3.13):

$$\|(\breve{\Phi}_N^{n+1})^2+\breve{\Phi}_N^{n+1}\breve{\phi}^{n+1}+(\breve{\phi}^{n+1})^2\|_\infty\leqslant 3M_0^2. \tag{3.24}$$

In terms of the first expansion part in (3.22), we observe a transformed representation for the nonlinear coefficient function:

$$\begin{aligned}&(\breve{\Phi}_N^{n+1})^2+\breve{\Phi}_N^{n+1}\breve{\phi}^{n+1}+(\breve{\phi}^{n+1})^2\\&\quad=(\breve{\Phi}_N^{n+1})^2+\breve{\Phi}_N^{n+1}(\breve{\Phi}_N^{n+1}-\breve{e}^{n+1})+(\breve{\Phi}_N^{n+1}-\breve{e}^{n+1})^2\\&\quad=3(\breve{\Phi}_N^{n+1})^2-3\breve{\Phi}_N^{n+1}\breve{e}^{n+1}+(\breve{e}^{n+1})^2\\&\quad=3(\Phi_N^{n+1})^2-3(\Phi_N^{n+1}+\breve{\Phi}_N^{n+1})(\Phi_N^{n+1}-\breve{\Phi}_N^{n+1})-3\breve{\Phi}_N^{n+1}\breve{e}^{n+1}+(\breve{e}^{n+1})^2.\end{aligned} \tag{3.25}$$

Meanwhile, for the nonlinear inner product associated with the numerically corrected terms, the following estimates are available.

We begin by bounding the inner product corresponding to the second term on the right-hand side of (3.25):

$$\begin{aligned}&\langle 3(\Phi_N^{n+1}+\breve{\Phi}_N^{n+1})(\Phi_N^{n+1}-\breve{\Phi}_N^{n+1})e^{n+1},e^{n+1}-e^n\rangle\\&\quad\leqslant 3(\|\Phi_N^{n+1}\|_\infty+\|\breve{\Phi}_N^{n+1}\|_\infty)\|\Phi_N^{n+1}-\breve{\Phi}_N^{n+1}\|_\infty\cdot\|e^{n+1}\|_2\cdot\|e^{n+1}-e^n\|_2\\&\quad\leqslant 3\cdot 2M_0\cdot\frac{1}{4}\Delta t\cdot\|e^{n+1}\|_2\cdot\|e^{n+1}-e^n\|_2\\&\quad=\frac{3}{2}M_0\Delta t\|e^{n+1}\|_2\cdot\|e^{n+1}-e^n\|_2\\&\quad\leqslant\frac{3M_0^2}{\gamma_0}\Delta t^2\|e^{n+1}\|_2^2+\frac{\gamma_0}{16}\|e^{n+1}-e^n\|_2^2\\&\quad\leqslant\Delta t\|e^{n+1}\|_2^2+\frac{\gamma_0}{16}\|e^{n+1}-e^n\|_2^2.\end{aligned} \tag{3.26}$$

Proceeding to the third term on the right-hand side of (3.25), we see that

$$\begin{aligned}\langle 3\breve{\Phi}_N^{n+1}\breve{e}^{n+1}e^{n+1},e^{n+1}-e^n\rangle&\leqslant 3\|\breve{\Phi}_N^{n+1}\|_\infty\cdot\|\breve{e}^{n+1}\|_\infty\cdot\|e^{n+1}\|_2\cdot\|e^{n+1}-e^n\|_2\\&\leqslant 3\cdot M_0\cdot\Delta t\cdot\|e^{n+1}\|_2\cdot\|e^{n+1}-e^n\|_2\\&=3M_0\Delta t\|e^{n+1}\|_2\cdot\|e^{n+1}-e^n\|_2\\&\leqslant\frac{12M_0^2}{\gamma_0}\Delta t^2\|e^{n+1}\|_2^2+\frac{\gamma_0}{16}\|e^{n+1}-e^n\|_2^2\\&\leqslant\Delta t\|e^{n+1}\|_2^2+\frac{\gamma_0}{16}\|e^{n+1}-e^n\|_2^2.\end{aligned} \tag{3.27}$$

For the last term on the right-hand side of (3.25), we have

$$\begin{aligned}\langle-(\breve{e}^{n+1})^2e^{n+1},e^{n+1}-e^n\rangle&\leqslant\|\breve{e}^{n+1}\|_\infty^2\cdot\|e^{n+1}\|_2\cdot\|e^{n+1}-e^n\|_2\\&\leqslant\Delta t^2\|e^{n+1}\|_2\cdot\|e^{n+1}-e^n\|_2\leqslant 4\Delta t^4\|e^{n+1}\|_2^2+\frac{\gamma_0}{16}\|e^{n+1}-e^n\|_2^2\\&\leqslant\Delta t\|e^{n+1}\|_2^2+\frac{\gamma_0}{16}\|e^{n+1}-e^n\|_2^2,\end{aligned} \tag{3.28}$$

in which the preliminary bounds (3.2), (3.7) and (3.8), as well as the *a priori* estimate (3.12), have been extensively used in the derivation. Subsequently, a substitution of (3.26)–(3.28) into (3.25) yields

$$\begin{aligned}&\langle((\breve{\Phi}_N^{n+1})^2+\breve{\Phi}_N^{n+1}\breve{\phi}^{n+1}+(\breve{\phi}^{n+1})^2)e^{n+1},e^{n+1}\rangle\\&\quad\geqslant\langle 3(\Phi_N^{n+1})^2e^{n+1},e^{n+1}-e^n\rangle-3\Delta t\|e^{n+1}\|_2^2-\frac{3\gamma_0}{16}\|e^{n+1}-e^n\|_2^2.\end{aligned} \tag{3.29}$$

Furthermore, a combination of (3.23) and (3.29) results in

$$\begin{aligned}&\langle(\breve{\Phi}_N^{n+1})^3-(\breve{\phi}^{n+1})^3,e^{n+1}-e^n\rangle\\&\quad\geqslant\langle 3(\Phi_N^{n+1})^2e^{n+1},e^{n+1}-e^n\rangle-3\Delta t\|e^{n+1}\|_2^2-\frac{7\gamma_0}{16}\|e^{n+1}-e^n\|_2^2\\&\qquad-\frac{18M_0^4}{\gamma_0}(\|e^{n+1}-2e^n+e^{n-1}\|_2^2+\|e^n-2e^{n-1}+e^{n-2}\|_2^2).\end{aligned}\tag{3.30}$$

On the other hand, in terms of the primary nonlinear error inner product, the following inequality holds:

$$\begin{aligned}\langle 3(\Phi_N^{n+1})^2e^{n+1},e^{n+1}-e^n\rangle&=\frac{3}{2}\langle\Phi_N^{n+1},(e^{n+1})^2-(e^n)^2+(e^{n+1}-e^n)^2\rangle\\&\geqslant\frac{3}{2}\langle(\Phi_N^{n+1})^2,(e^{n+1})^2-(e^n)^2\rangle\\&=\frac{3}{2}(\langle(\Phi_N^{n+1})^2,(e^{n+1})^2\rangle-\langle(\Phi_N^{n+1})^2,(e^n)^2\rangle).\end{aligned}\tag{3.31}$$

To make this quantity the difference of two recursive terms, we observe the following estimate:

$$\|(\Phi_N^{n+1})^2-(\Phi_N^n)^2\|_\infty\leqslant(\|\Phi_N^{n+1}\|_\infty+\|\Phi_N^n\|_\infty)\|\Phi_N^{n+1}-\Phi_N^n\|_\infty\leqslant 2C^*\cdot C^*\Delta t=2(C^*)^2\Delta t\tag{3.32}$$

and

$$\begin{aligned}|\langle(\Phi_N^{n+1})^2,(e^n)^2\rangle-\langle(\Phi_N^n)^2,(e^n)^2\rangle|&=|\langle(\Phi_N^{n+1})^2-(\Phi_N^n)^2,(e^n)^2\rangle|\\&\leqslant\|(\Phi_N^{n+1})^2-(\Phi_N^n)^2\|_\infty\cdot\|e^n\|_2^2\\&\leqslant 2(C^*)^2\Delta t\|e^n\|_2^2.\end{aligned}\tag{3.33}$$

Going back (3.31), we arrive at

$$\langle 3(\Phi_N^{n+1})^2e^{n+1},e^{n+1}-e^n\rangle\geqslant\frac{3}{2}(\langle(\Phi_N^{n+1})^2,(e^{n+1})^2\rangle-\langle(\Phi_N^n)^2,(e^n)^2\rangle)-2(C^*)^2\Delta t\|e^n\|_2^2,\tag{3.34}$$

and its combination with (3.30) leads to the nonlinear error estimate

$$\begin{aligned}&\langle(\breve{\Phi}_N^{n+1})^3-(\breve{\phi}^{n+1})^3,e^{n+1}-e^n\rangle\\&\quad\geqslant\frac{3}{2}(\langle(\Phi_N^{n+1})^2,(e^{n+1})^2\rangle-\langle(\Phi_N^n)^2,(e^n)^2\rangle)-3\Delta t\|e^{n+1}\|_2^2-2(C^*)^2\Delta t\|e^n\|_2^2\\&\qquad-\frac{7\gamma_0}{16}\|e^{n+1}-e^n\|_2^2-\frac{18M_0^4}{\gamma_0}(\|e^{n+1}-2e^n+e^{n-1}\|_2^2+\|e^n-2e^{n-1}+e^{n-2}\|_2^2).\end{aligned}\tag{3.35}$$

The bound for the right-hand side term of (3.14) associated with the truncation error is straightforward:

$$\begin{aligned}\langle(-\Delta_N)^{-1}e^{n+1}-e^n,\tau_0^{n+1}\rangle&\leqslant\|e^{n+1}-e^n\|_{-1,N}\cdot\|\tau_0^{n+1}\|_{-1,N}\\&\leqslant\frac{1}{12\Delta t}\|e^{n+1}-e^n\|_{-1,N}^2+3\Delta t\|\tau_0^{n+1}\|_{-1,N}^2.\end{aligned}\tag{3.36}$$

Therefore, a substitution of (3.15)–(3.17), (3.21), (3.35) and (3.36) into (3.14) results in

$$\begin{aligned}&\frac{1}{\Delta t}\left(\frac{5}{6}\|e^{n+1}-e^n\|_{-1,N}^2-\frac{7}{12}\|e^n-e^{n-1}\|_{-1,N}^2-\frac{1}{6}\|e^{n-1}-e^{n-2}\|_{-1,N}^2\right)\\&\quad+\frac{\gamma_0}{2}(\|e^{n+1}\|_2^2-\|e^n\|_2^2)+\frac{A\Delta t}{2}(\|\nabla_N(e^{n+1}-e^n)\|_2^2-\|\nabla_N(e^n-e^{n-1})\|_2^2)\\&\quad+\frac{3}{2}(\langle(\Phi_N^{n+1})^2,(e^{n+1})^2\rangle-\langle(\Phi_N^n)^2,(e^n)^2\rangle)+\frac{\gamma_0}{16}\|\phi^{n+1}-\phi^n\|_2^2\\&\quad+\frac{7}{12\Delta t}\|e^{n+1}-2e^n+e^{n-1}\|_{-1,N}^2+\frac{A\Delta t}{2}\|\nabla_N(e^{n+1}-2e^n+e^{n-1})\|_2^2\\&\qquad\leqslant(3+12C_2\varepsilon^4)\Delta t\|e^{n+1}\|_2^2+2(C^*)^2\Delta t\|e^n\|_2^2+3\Delta t\|\tau_0^{n+1}\|_{-1,N}^2\\&\qquad\quad+\left(\frac{18M_0^4}{\gamma_0}+24C_2\varepsilon^4\Delta t\right)(\|e^{n+1}-2e^n+e^{n-1}\|_2^2+\|e^n-2e^{n-1}+e^{n-2}\|_2^2).\end{aligned}$$

A similar estimate can be derived with the help of the Cauchy-Schwarz inequality:

$$\begin{aligned}&\frac{7}{12\Delta t}\|e^{n+1}-2e^n+e^{n-1}\|_{-1,N}^2+\frac{A\Delta t}{2}\|\nabla_N(e^{n+1}-2e^n+e^{n-1})\|_2^2\\&\geqslant\left(\frac{7}{6}A\right)^{\frac{1}{2}}\|e^{n+1}-2e^n+e^{n-1}\|_2^2.\end{aligned}\tag{3.37}$$

Subsequently, the following quantity is introduced to facilitate the estimation:

$$\begin{aligned}F^{n+1}:=&\frac{3}{2}\langle(\Phi_N^{n+1})^2,(e^{n+1})^2\rangle+\frac{\gamma_0}{2}\|e^{n+1}\|_2^2+\frac{3}{4\Delta t}\|\phi^{n+1}-\phi^n\|_{-1,N}^2\\&+\frac{1}{6\Delta t}\|\phi^n-\phi^{n-1}\|_{-1,N}^2+\left(\frac{7}{24}A\right)^{\frac{1}{2}}\|\phi^{n+1}-2\phi^n+\phi^{n-1}\|_2^2\\&+\frac{A\Delta t}{2}\|\nabla_N(\phi^{n+1}-\phi^n)\|_2^2.\end{aligned}\tag{3.38}$$

Going back (3.37), we arrive at

$$F^{n+1}-F^n\leqslant(3+12C_2\varepsilon^4)\Delta t\|e^{n+1}\|_2^2+2(C^*)^2\Delta t\|e^n\|_2^2+3\Delta t\|\tau_0^{n+1}\|_{-1,N}^2\tag{3.39}$$

under the constraint (3.3), in which the following bounds have been applied:

$$24C_2\varepsilon^4\Delta t\leqslant 1,\quad \frac{18M_0^4}{\gamma_0}+1\leqslant\left(\frac{7}{24}A\right)^{\frac{1}{2}}=\frac{1}{2}\left(\frac{7}{6}A\right)^{\frac{1}{2}}.$$

Moreover, by an obvious fact that $\|e^k\|_2^2\leqslant 2\gamma_0^{-1}F^k$, for any $k\geqslant 0$, we get

$$F^{n+1}-F^n\leqslant(6+24C_2\varepsilon^4)\gamma_0^{-1}\Delta tF^{n+1}+4(C^*)^2\gamma_0^{-1}\Delta tF^n+3\Delta t\|\tau_0^{n+1}\|_{-1,N}^2.\tag{3.40}$$

Consequently, an application of the discrete Gronwall inequality leads to the desired convergence estimate

$$F^{n+1}\leqslant\hat{C}(\Delta t^6+h^{2m}),\tag{3.41}$$

due to the fact that $\|\tau_0^{n+1}\|_{-1,N}\leqslant C(\Delta t^3+h^m)$. As a result, it is observed that

$$\|e^{n+1}\|_2\leqslant(2\gamma_0^{-1})^{\frac{1}{2}}\hat{C}(\Delta t^3+h^m)\leqslant\Delta t^{\frac{11}{4}}+h^{m-1},\tag{3.42}$$

so that the *a priori* assumption (3.11) has been recovered at time instant t^{n+1}. In turn, the analysis can be carried out in an induction style. This completes the error estimate, and the proof of Theorem 3.1 is complete.

Remark 3.3. It is worth highlighting the choice of the test function $(-\Delta_N)^{-1}(e^{n+1}-e^n)$ here. A standard error analysis for Cahn-Hilliard-type equations typically employs the error function itself, i.e., $(-\Delta_N)^{-1}e^{n+1}$, to derive an H^{-1} norm estimate; see the related work [23] for the first-order scheme. However, even for the second-order accurate (in temporal accuracy order) scheme, such an analytic approach faces a serious difficulty in the theoretical derivation of the error estimate, due to the lack of diffusion power in the nonlocal gradient flow model; the related arguments have been presented for the BDF2 [24] and Crank-Nicolson style [25] algorithms. In terms of the third-order BDF3 scheme, a direct application of the test function $(-\Delta_N)^{-1}e^{n+1}$ fails in the case of the standard Cahn-Hilliard equation (with a local diffusion operator), which comes from challenges associated with the long temporal stencil involving multiple previous time steps; see also the original literature [27] and a few applications to various gradient flow models [8, 17]. Therefore, for the BDF3 scheme applied to the nonlocal Cahn-Hilliard equation, the test function $(-\Delta_N)^{-1}(e^{n+1}-e^n)$ is the appropriate choice. By adopting the discrete temporal derivative as the test function, we effectively follow the energy stability analysis of the scheme. This approach utilizes the gradient flow structure, allowing us to construct a modified energy functional for the error.

As proved in Proposition 2.3, the energy stability for the numerical scheme (2.4) is valid under the condition (2.6). In fact, the $\|\cdot\|_\infty$ bound (3.13) for the numerical solution $\breve{\phi}^{n+1} = 3\phi^n - 3\phi^{n-1} + \phi^{n-2}$ is available. In addition, the convergence analysis reveals that, such an $\|\cdot\|_\infty$ bound (3.13) for the numerical solution ϕ^{n+1} also holds:

$$\|e^{n+1}\|_\infty \leqslant \frac{C\|e^{n+1}\|_2}{h^{\frac{3}{2}}} \leqslant C\hat{C}(\Delta t^{\frac{5}{4}} + h^{m-\frac{5}{2}}) \leqslant \frac{1}{8}\Delta t \leqslant 1,$$

so that

$$\|\phi^{n+1}\|_\infty = \|\Phi_N^{n+1} - e^{n+1}\|_\infty \leqslant \|\Phi_N^{n+1}\|_\infty + \|e^{n+1}\|_\infty \leqslant C^* + 1 = M_0. \tag{3.43}$$

In more detail, we observe that (3.3) is a stronger constraint (for A) than (2.6). The following corollary provides a theoretical justification of the energy stability.

Corollary 3.4. *Under the assumptions of Theorem* 3.1*, the modified energy stability, i.e.,* $\tilde{E}_N(\phi^{n+1}, \phi^n, \phi^{n-1}) \leqslant \tilde{E}_N(\phi^n, \phi^{n-1}, \phi^{n-2})$*, is valid under the constraint* (3.3) *for the regularization parameter A, combined with a trivial constraint for* $\Delta t : 24C_2\varepsilon^4\Delta t \leqslant \min(1, \gamma_0)$.

4 The numerical experiment results

In this section, we present several numerical experiments using the proposed stabilized BDF3 scheme (2.4) to solve the NCH equation (1.3). Following the reference example in [9], we employ a family of Gaussian-type kernels parameterized by a positive constant δ, defined as follows:

$$J(\boldsymbol{x}) = \frac{4}{\pi^{d/2}\delta^{d+2}} e^{-|\boldsymbol{x}|^2/\delta^2}, \quad \boldsymbol{x} \in \mathbb{R}^d, \quad \delta > 0. \tag{4.1}$$

As the parameter δ approaches zero, the nonlocal Cahn-Hilliard model with this Gaussian kernel converges to the classical Cahn-Hilliard model. This convergence occurs because, for any $\phi \in C^\infty(\Omega)$ and for any $\boldsymbol{x} \in \Omega$, we obtain $\mathcal{L}\phi(\boldsymbol{x}) \to -\Delta\phi(\boldsymbol{x})$ as $\delta \to 0$. Furthermore, it is worth noting that the steady-state solution of the nonlocal Cahn-Hilliard equation is continuous when $\delta \leqslant 2\varepsilon$.

Remark 4.1. In this work, the Gaussian kernel is selected primarily for its smoothness, which is suitable for the Fourier pseudo-spectral spatial discretization. It is noticed that the proposed BDF3 time-stepping scheme is general, and the theoretical analysis can be extended to other gradient flow models with smooth convolution kernels. On the other hand, it is noticed that a singular convolution kernel (such as the one associated with the regular Laplacian operator) usually leads to a stronger diffusion power and much sharper regularity for the PDE solution, and the corresponding numerical design and numerical analysis can follow the ones for the standard Cahn-Hilliard equation. This work is primarily focused on a smooth convolution kernel, where the lack of diffusion power and higher-order Sobolev estimates make the corresponding analysis much more challenging. If a singular convolution kernel is considered, a more appropriate approach would be following the framework of the standard Cahn-Hilliard equation, in terms of numerical design and analysis.

4.1 Convergence rate in time

In this example, we conduct a numerical convergence analysis for the stabilized BDF3 scheme on the periodic domain $\Omega = (-1, 1)^2$. The initial condition is given by

$$\phi_0(x, y) = 0.5\sin(\pi x)\sin(\pi y) + 0.1.$$

We use the kernel function described in (4.1) with two different parameters: $\varepsilon^2 = 0.1$ and $\varepsilon^2 = 0.01$. For each ε, three corresponding kernel parameters, i.e., $\delta^2 \in \{\varepsilon^2, 2\varepsilon^2, 3\varepsilon^2\}$, are considered. The stabilization constant is taken as $A = 10$. Numerical solutions are computed at the final time $t = 0.1$.

The Fourier spectral collocation discretization over 1024×1024 uniform mesh is taken, which ensures that spatial errors are negligible compared to temporal ones. We perform temporal refinement studies

with a sequence of time step sizes $\Delta t = 2^{-k}\Delta_0$ for $k = 1, 2, \ldots, 8$, where $\Delta_0 = 0.005$ is the base time step. The solution obtained with the smallest time step $\Delta t = 2^{-8}\Delta_0/5$ is used as the reference solution to measure numerical errors. Figure 1 displays the discrete ℓ^2 errors in terms of temporal step size for different values of ε and δ. The error profiles clearly indicate the expected third-order temporal convergence rates.

Finally, we investigate the sensitivity of the numerical accuracy and convergence order with respect to the stabilization parameter A. While the theoretical analysis requires a sufficiently large A for stability, it is crucial to verify that the parameter choice does not reduce the temporal accuracy order. We conduct the convergence test with $\epsilon^2 = \delta^2 = 0.1$, using varying stabilization parameter values of $2, 5, 10, 20$ and 50. Figure 1(c) displays the ℓ^2 error curves for these computations. The results indicate that the third-order convergence rate is generally preserved across the tested values. It is observed that increasing A leads to a slight increase in the error magnitude due to the larger artificial diffusion introduced by the regularization term. Conversely, while $A = 2$ yields the smallest numerical error, the convergence curve exhibits a slight irregularity, implying that the stabilization might be marginally insufficient. This demonstrates that the scheme is numerically robust, and a moderate parameter value (e.g., $A = 5$ or $A = 10$) offers an optimal balance between stability and accuracy.

4.2 Simulation results of the coarsening dynamics

Numerical simulations are conducted over a square domain $\Omega = (-2\pi, 2\pi)^2$ with periodic boundary conditions to study phase separation dynamics. The initial condition consists of random perturbations uniformly distributed in the range of $[-0.1, 0.1]$ at each grid point over a uniform spatial mesh. A two-stage time-stepping distribution approach is adopted, where $\Delta t = 0.0005$ for $t \in [0, 1000)$ and $\Delta t = 0.01$ for $t \in [1000, 10000)$, with a stabilization parameter $A = 5$.

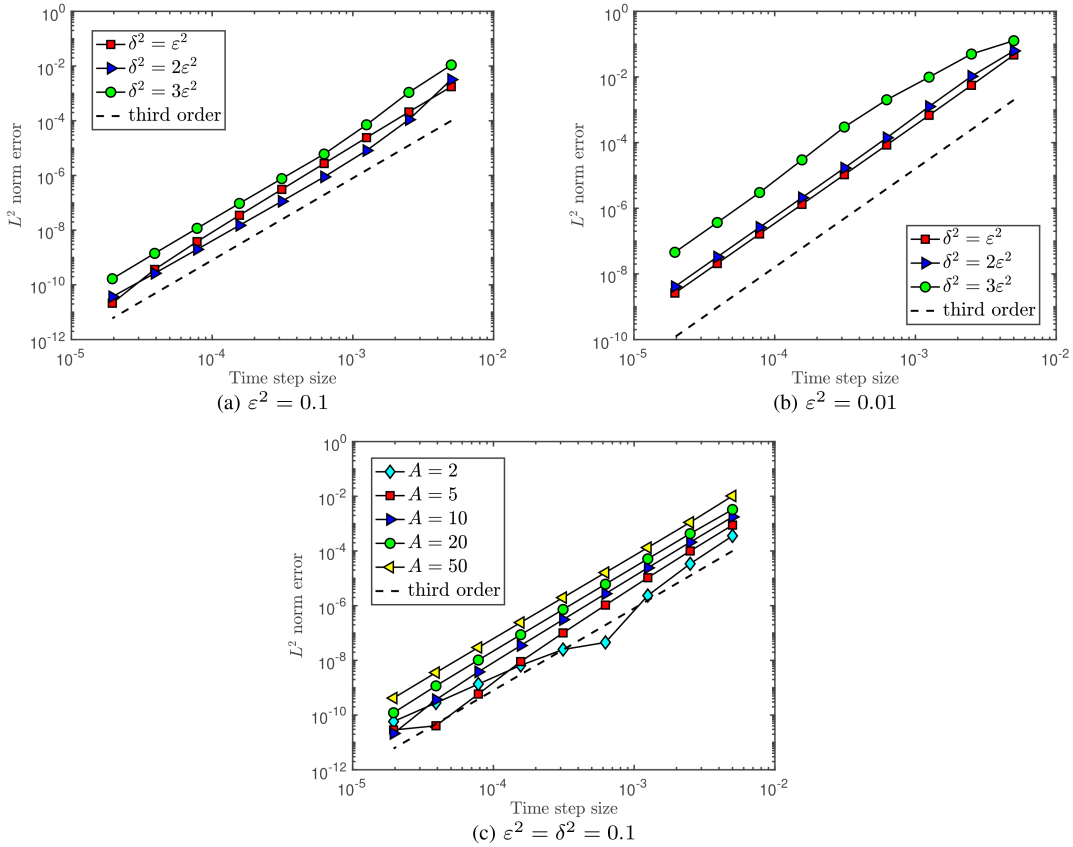

(a) $\varepsilon^2 = 0.1$ (b) $\varepsilon^2 = 0.01$

(c) $\varepsilon^2 = \delta^2 = 0.1$

Figure 1 (Color online) Temporal convergence test of the stabilized BDF3 scheme

Case 1 (Fixed δ and varying ε). With $\delta = 0.05$ and spatial resolution $N = 256$, simulations are performed for a sequence of ε values, from 0.08 to 0.04. Figure 2 shows the snapshot plots of the numerical solution with $\varepsilon = 0.04$, at selected time instants $t = 1, 3, 10, 100, 400, 5000$. The system transitions rapidly from disordered initial states to ordered patterns, and reaches a steady configuration near $t = 5000$. The energy evolution curves for $\varepsilon = 0.08, 0.06, 0.04$ in Figure 3(a) align closely with the theoretical $t^{-1/3}$ scaling law [9], as demonstrated by a direct comparison with the reference line $Ct^{-1/3}$. It is noticed that the energy profiles plotted in Figure 3 correspond to the original discrete free energy E_N defined in (1.1).

Case 2 (Fixed ε and varying δ). With a fixed $\varepsilon = 0.09$, the parameter δ^2 is increased from ε^2 to $3\varepsilon^2$. Figure 3(b) plots the corresponding energy decay profiles. The numerical results have consistently indicate the theoretical $t^{-1/3}$ energy decay rate across all tested values of δ.

4.3 Simulation for the case of $\gamma_0 < 0$

In this subsection, we present a numerical example, where the diffusivity condition (1.4) is violated. As discussed in Section 2, the condition $\gamma_0 > 0$ is required for the well-posedness of the NCH equation.

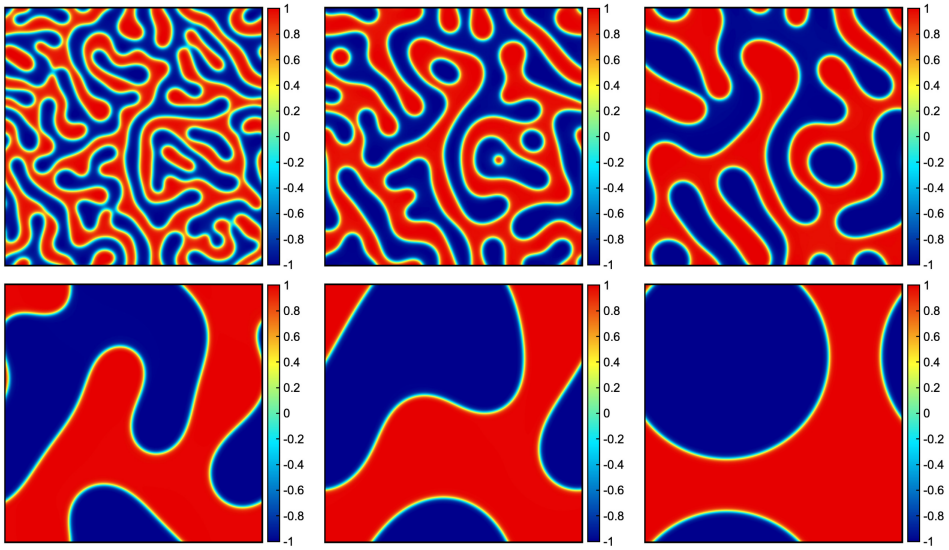

Figure 2 (Color online) Snapshot plots are taken at $t = 1,\ 3,\ 10,\ 100,\ 200,\ 5000$, with $\varepsilon = \delta = 0.09$ in the coarsening process simulation. The vertical colorbar on the right represents the order parameter ϕ, where the numerical scale ranges from 0 to 1.

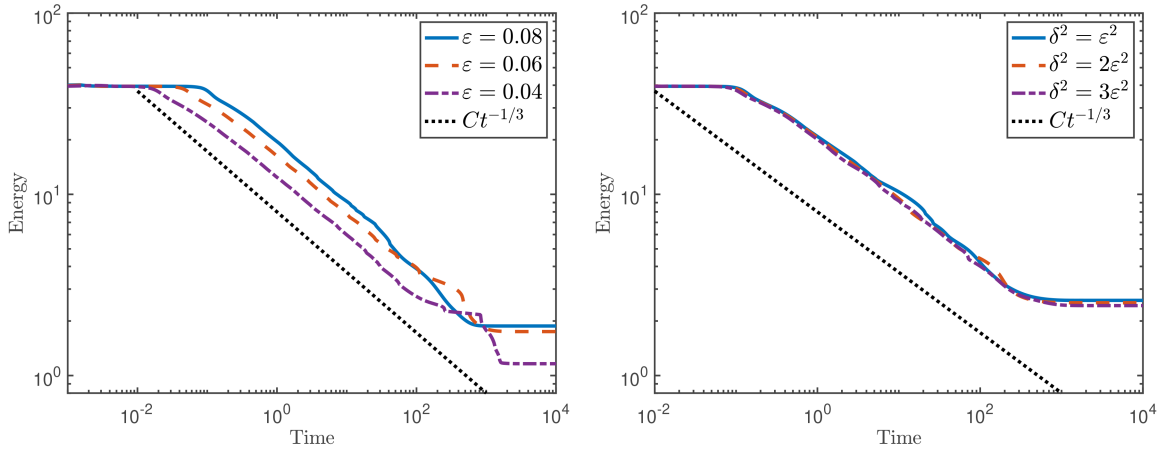

(a) $\delta = 0.05$ (b) $\varepsilon = 0.09$

Figure 3 (Color online) Original energy evolutions for (a) Case 1 with $\delta = 0.05$ and (b) Case 2 with $\varepsilon = 0.09$

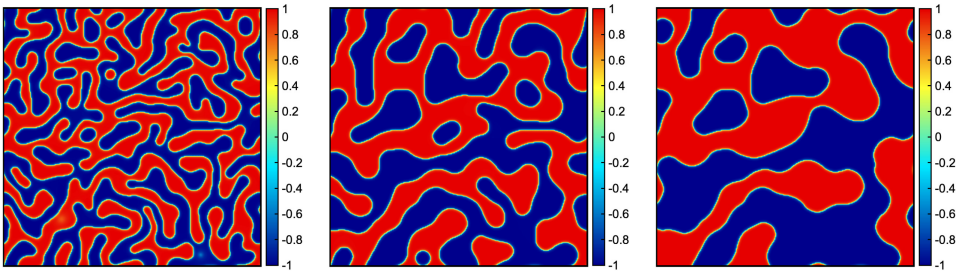

Figure 4 (Color online) Snapshot plots are taken at $t = 2,\ 20,\ 200$ with $\varepsilon = 0.04$, $\delta = 0.08$ in the coarsening process simulation. The vertical colorbar on the right represents the order parameter ϕ, where the numerical scale ranges from 0 to 1.

To investigate the solution behavior when this condition fails, we set the same initial and boundary conditions as in Subsection 4.2 with $\epsilon = 0.04$ and $\delta = 0.08$. This choice implies that $\gamma_0 < 0$. Figure 4 displays the numerical solution snapshots at $t = 2, 20, 200$. Unlike the smooth phase transitions observed in the previous examples, the solution here exhibits clear singular behaviors, characterized by sharp, non-smooth interfaces. This result numerically confirms that the condition (1.4) is essential for maintaining the regularity of the solution.

5 Some concluding remarks

In this paper, we propose and analyze a third-order (in time) stabilized numerical scheme for the nonlocal Cahn-Hilliard equation, with the Fourier pseudo-spectral spatial discretization. The BDF3 is used as temporal discretization, combined with an explicit extrapolation for both the nonlinear term and the convolution part, as well as a third-order accurate Douglas-Dupont regularization. In particular, the expansive concave term is combined with the constant multiple part in the nonlocal diffusion operator expansion part, and the standard BDF3 temporal discretization is applied to this combined term. A careful energy estimate gives a rough dissipation analysis in terms of a modified energy functional, in which a lower bound of the artificial regularization parameter is derived in terms of a maximum norm assumption of the numerical solution. In addition, the convergence analysis and error estimate turns out to be necessary to recover this functional bound, with the help of an alternate numerical error test function, in the form of a discrete temporal derivative. This in turn justifies the modified energy stability result, with the induction style analysis accomplished. A few computational results are presented to verify the theoretical analysis and the robustness of the proposed numerical method.

Acknowledgements This work was supported by National Natural Science Foundation of China (Grant No. 12371385) and National Science Foundation of USA (Grant Nos. DMS-2012269 and DMS-2309548).

References

1 Bates P W. On some nonlocal evolution equations arising in materials science. Nonlinear Anal Real World Appl, 2006, 48: 13–52
2 Bates P W, Brown S, Han J. Numerical analysis for a nonlocal Allen-Cahn equation. Int J Numer Anal Model, 2009, 6: 33–49
3 Bates P W, Han J. The Neumann boundary problem for a nonlocal Cahn-Hilliard equation. J Differential Equations, 2005, 212: 235–277
4 Bates P W, Han J. The Dirichlet boundary problem for a nonlocal Cahn-Hilliard equation. J Math Anal Appl, 2005, 311: 289–312
5 Bates P W, Han J, Zhao G. On a nonlocal phase-field system. Nonlinear Anal, 2006, 64: 2251–2278
6 Cahn J W, Hilliard J E. Free energy of a nonuniform system. I. Interfacial free energy. J Chem Phys, 1958, 28: 258–267
7 Chen W, Li W, Wang C, et al. Energy stable higher-order linear ETD multi-step methods for gradient flows: Application to thin film epitaxy. Res Math Sci, 2020, 7: 13

8 Cheng K, Wang C, Wise S M, et al. A third order accurate in time, BDF-type energy stable scheme for the Cahn-Hilliard equation. Numer Math Theory Methods Appl, 2022, 15: 2, 279–303

9 Du Q, Ju L, Li X, et al. Stabilized linear semi-implicit schemes for the nonlocal Cahn-Hilliard equation. J Comput Phys, 2018, 363: 39–54

10 Du Q, Ju L, Li X, et al. Maximum principle preserving exponential time differencing schemes for the nonlocal Allen-Cahn equation. SIAM J Numer Anal, 2019, 57: 875–898

11 Du Q, Tao Y, Tian X, et al. Asymptotically compatible discretization of multidimensional nonlocal diffusion models and approximation of nonlocal Green's functions. IMA J Numer Anal, 2019, 39: 607–625

12 Fife P. Some nonclassical trends in parabolic and Parabolic-Like evolutions. In: Trends in Nonlinear Analysis. Berlin: Springer, 2003, 153–191

13 Fu Y, Zhang G, Qian X, et al. Mass-, and energy-preserving sine pseudo-spectral schemes with high-accuracy for the coupled nonlinear Schrödinger equation. Adv Appl Math Mech, 2025, 17: 1430–1455

14 Guan Z, Lowengrub J S, Wang C. Convergence analysis for second-order accurate schemes for the periodic nonlocal Allen-Cahn and Cahn-Hilliard equations. Math Methods Appl Sci, 2017, 40: 6836–6863

15 Guan Z, Lowengrub J S, Wang C, et al. Second order convex splitting schemes for periodic nonlocal Cahn-Hilliard and Allen-Cahn equations. J Comput Phys, 2014, 277: 48–71

16 Guan Z, Wang C, Wise S M. A convergent convex splitting scheme for the periodic nonlocal Cahn-Hilliard equation. Numer Math, 2014, 128: 377–406

17 Hao Y, Huang Q, Wang C. A third order BDF energy stable linear scheme for the no-slope-selection thin film model. Commun Comput Phys, 2021, 29: 905–929

18 Li C, Tang L, Zhou J. Numerical analysis of stabilized second order semi-implicit finite element methods for the phase-field equations. Adv Appl Math Mech, 2024, 16: 667–691

19 Li D, Qiao Z H. On the stabilization size of semi-implicit Fourier-spectral methods for 3D Cahn-Hilliard equations. Commun Math Sci, 2017, 15: 1489–1506

20 Li D, Qiao Z H. On second order semi-implicit Fourier spectral methods for 2D Cahn-Hilliard equations. J Sci Comput, 2017, 70: 301–341

21 Li D, Qiao Z H, Tang T. Characterizing the stabilization size for semi-implicit Fourier-spectral method to phase field equations. SIAM J Numer Anal, 2016, 54: 1653–1681

22 Li X, Liu Z, Shen J, et al. On a class of higher-order fully decoupled schemes for the Cahn-Hilliard-Navier-Stokes system. J Sci Comput, 2025, 103: 1–28

23 Li X, Qiao Z H, Wang C. Convergence analysis for a stabilized linear semi-implicit numerical scheme for the nonlocal Cahn-Hilliard equation. Math Comp, 2021, 90: 171–188

24 Li X, Qiao Z H, Wang C. Stabilization parameter analysis of a second-order linear numerical scheme for the nonlocal Cahn-Hilliard equation. IMA J Numer Anal, 2023, 43: 1089–1114

25 Li X, Qiao Z H, Wang C. Double stabilizations and convergence analysis of a second-order linear numerical scheme for the nonlocal Cahn-Hilliard equation. Sci China Math, 2024, 67: 187–210

26 Liao H, Tang T, Wang X, et al. A class of refined implicit-explicit Runge-Kutta methods with robust time adaptability and unconditional convergence for the Cahn-Hilliard model. Math Comp, 2026, 95: 1293–1325

27 Liu J. Simple and efficient ALE methods with provable temporal accuracy up to fifth order for the Stokes equations on time varying domains. SIAM J Numer Anal, 2013, 51: 743–772

28 Shen J, Tang T, Wang L. Spectral Methods: Algorithms, Analysis and Applications. Heidelberg: Springer, 2011

29 Shen J, Yang X. Numerical approximations of Allen-Cahn and Cahn-Hilliard equations. Discrete Contin Dyn Syst, 2010, 28: 1669–1691

30 Teng X, Zhang H. A third-order energy stable exponential-free Runge-Kutta framework for the nonlocal Cahn-Hilliard equation. J Sci Comput, 2025, 103: 74

31 Tian X, Du Q. Asymptotically compatible schemes and applications to robust discretization of nonlocal models. SIAM J Numer Anal, 2014, 52: 1641–1665

32 Trefethen L N. Spectral Methods in MATLAB. Philadelphia: SIAM, 2000

33 Yang X, Zhao J. Efficient linear schemes for the nonlocal Cahn-Hilliard equation of phase field models. Comput Phys Commun, 2019, 235: 234–245

34 Zhou K, Du Q. Mathematical and numerical analysis of linear peridynamic models with nonlocal boundary conditions. SIAM J Numer Anal, 2010, 48: 1759–1780